Naked-eye ghost imaging via photoelectric feedback

Gao Wang (王 高)[1], Huaibin Zheng (郑淮斌)[1,2,*], Zhiguo Tang (汤志国)[1], Yuchen He (贺雨晨)[1,2], Yu Zhou (周 宇)[3], Hui Chen (陈 辉)[1], Jianbin Liu (刘建彬)[1,2], Yuan Yuan (袁 园)[1], Fuli Li (李福利)[3], and Zhuo Xu (徐 卓)[1,2]

[1]*Key Laboratory of Multifunctional Materials and Structures, Ministry of Education, School of Electronic Science and Engineering, Xi'an Jiaotong University, Xi'an 710049, China*

[2]*Electronic Materials Research Laboratory, Key Laboratory of the Ministry of Education & International Center for Dielectric Research, School of Electronic Science and Engineering, Xi'an Jiaotong University, Xi'an 710049, China*

[3]*Key Laboratory for Nonequilibrium Synthesis and Modulation of Condensed Matter, Ministry of Education, Department of Applied Physics, Xi'an Jiaotong University, Xi'an 710049, China*

**Corresponding author: huaibinzheng@xjtu.edu.cn*

Received February 3, 2020; accepted May 27, 2020; posted online July 21, 2020

A new architecture, naked-eye ghost imaging via photoelectric feedback, is developed that avoids computer algorithm processing. Instead, the proposed scheme uses a photoelectric feedback loop to first realize the correlation (multiplication) process of the traditional ghost imaging system. Then, the vision persistence effect of the naked eye is exploited to implement the integral process and to generate negative images. Two kinds of feedback circuits, the digital circuit and the analog circuit, are presented that can achieve a feedback operation. Based on this design, high-contrast real-time imaging of moving objects is obtained via a special pattern-scanning architecture on a low-speed light-modulation mask.

Keywords: ghost imaging; naked-eye; photoelectric feedback.
doi: 10.3788/COL202018.091101.

Since its inception in the 1990s, ghost imaging has intrigued researchers due to its novel physical peculiarities and its potential possible applications. The typical ghost imaging setup consists of two correlated optical beams propagating in distinct paths and impinging on two spatially-separated photodetectors. The signal beam interacts with an object and then is received by a single-pixel (bucket) detector without a spatial resolution, whereas the reference beam goes through the other independent path and impinges on a spatial distribution detector, like a charge-coupled device (CCD) without interacting with the object. Even though information from either one of the detectors used for the acquisition does not yield an image, the image can be obtained by cross-correlating signals from the bucket detector and the CCD.

The first ghost imaging, utilizing two-photon quantum entanglement, is reported by Pittman *et al.*[1]. Later, it was demonstrated that ghost imaging could be implemented with pseudo-thermal sources[2–5] and thermal light[6]. In addition, computational ghost imaging with an improved setup was proposed by Shapiro[7,8], where the reference beam was instead from a computed field pattern. With the development of ghost imaging, this concept has been extended to domains beyond the usual optical domain mentioned above and outside of the capture of the spatial properties of light. Recently, it has been demonstrated with X-rays[9–12], atoms[13], and even electrons[14], as well as temporal ghost imaging[15–21].

Generally, up to now, the popular way to get the output image is routinely reconstructed by a computer algorithm from the acquired data[22,23]. This situation was developed in a new way to get the reconstructed image with the properties of naked-eye ghost imaging[24,25]. However, from both the theoretical and experimental results at that time, a low-contrast image is the main obstacle to push this idea closer to practical applications, since the image is immersed in the reference light beam. Recently, we have solved this problem via all-optical process and the persistence of vision with a special pattern-scanning architecture[26].

Here, based on our preliminary work, an alternatively novel naked-eye ghost imaging scheme avoiding computer algorithm processing is proposed that will promote the convenience of ghost imaging. In detail, a photoelectric feedback loop is used to link the bucket detector and the light source, where the intensity of the light source is modulated by each output current value of the bucket detector. That is to say, the traditional ghost imaging's correlation (multiplication) process between the output current value of the bucket detector and the corresponding value of the intensity distribution of the reference beam is realized by this new photoelectric feedback loop method. It is important to recognize that there is inverse correlation in our work. Meanwhile, the vision persistence effect is used to implement the integral process and to generate negative images observed by naked eyes. In principle, all photosensitive material with the vision persistence effect can be effective to show the imaging result for this integral imaging process.

To realize high-contrast naked-eye ghost imaging, one of the challenges is overcoming the background introduced by the reference beam, since the image is immersed in the

reference light beam. Toward this end, a special pattern-scanning architecture on a low-speed light-modulation mask is used that enables high-resolution imaging with lower-order Hadamard vectors and also boosts the imaging speed.

Moreover, two kinds of feedback circuits, the digital circuit and the analog circuit, are presented that can achieve a high-speed feedback operation on the light intensity. With this approach, we demonstrate high-contrast real-time imaging for moving objects. Our work opens a new way to utilize ghost imaging and can be applied to those recently developed ghost imaging methods with the usual optical domain, X-rays, atoms and electrons, or the field of LIDAR.

The schematic diagram of the naked-eye ghost imaging system via photoelectric feedback is shown in Fig. 1.

First, the red laser beam is modulated by a rotating light-modulation mask.

Then, the modulated light pattern is divided into two beams, the reference beam and the signal beam. The reference beam, illuminating the screen, is used to achieve naked-eye imaging, while the signal beam illuminates and interacts with objects (letters "X", "J", "T", and "U"), each with 35×35 pixels. After transmitting the objects, the beam is collected by a bucket detector comprising a collecting lens and a single-pixel photodetector.

After this, the output signal of the bucket detector is processed via a feedback circuit to modulate the laser intensity. Namely, the intensity of the patterns changes inversely with the matching level between the pattern and the object.

Over all, once a group of patterns were completed during the vision persistence time, a negative image could be observed by looking at the screen.

In this work, a CCD camera is used to mimic the vision persistence effect of human eyes, a visual stimulus that continues to be experienced for a limited time after its offset, and 0.2 s is set as the exposure time of the CCD[26].

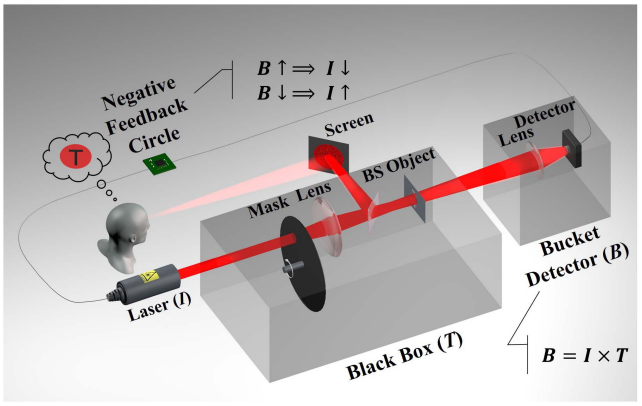

Fig. 1. Schematic diagram of the naked-eye ghost imaging system, including a laser device (I), block box (T), bucket detector (B), feedback loop, and naked-eye imaging. The block box with a transmissivity T_i is comprised of a mask, a lens, a BS, and an object.

At this point, a high-contrast real-time image will be observed by the photosensitive component.

The differences from the typical ghost imaging setup are that a photoelectric feedback loop is used to link the bucket detector and the light source, and the negative image can be observed directly by the naked eye at the position where the spatial distribution detector of the typical ghost imaging is placed. To understand such a naked-eye ghost imaging process simply, the imaging mechanism is shown in the following.

The total setup can be divided into four parts: laser source, black box, bucket detector, and negative feedback circle. Initially, the laser beam with intensity I_i goes through a black box (between the laser source and the bucket detector) with a transmissivity T_i that denotes the transmissivity from the light source (before being modulated by a rotating mask) to the final detection, and then is collected by a bucket detector, as shown in Fig. 1. By the way, T_i can be seen as a scale value (laser energy input) to scale value (detected output) function, and stands for the transmissivity of the so-called black box (comprising a rotating mask, a lens, a beam splitter, and objects). Thus, the output value B_i of the bucket detector is given by

$$B_i = I_i \times T_i. \tag{1}$$

Then, with this result, the electro-optic modulation function $f(B_i)$ is used to modulate the laser, and the intensity I_{i+1} is

$$I_{i+1} = f(B_i) = f(I_i \times T_i), \tag{2}$$

where the subscript $(i+1)$ represents the next moment after the ith moment. Therefore, from the aspect of statistics or steady state, it finally develops from Eq. (2) to Eq. (3), and it can be rewritten as

$$I = f(B) = f(I \times T). \tag{3}$$

The negative feedback circuit has the characteristic

$$\frac{\mathrm{d}f(B)}{\mathrm{d}B} < 0. \tag{4}$$

When taking Eq. (1), Eq. (3), and Eq. (4) into consideration, Eq. (5) can be derived. This means that the laser intensity I is a decreasing function of T:

$$\frac{\mathrm{d}I}{\mathrm{d}T} = \frac{\mathrm{d}f(B)}{\mathrm{d}B}\frac{\mathrm{d}B}{\mathrm{d}T} = \frac{\mathrm{d}f(B)}{\mathrm{d}B} I < 0. \tag{5}$$

Without the feedback loop, this system would degenerate into the traditional ghost imaging system, and the intensity of the light source would be a constant value. For simplicity, we take the constant value as 1. Thus, $I_2(t_i)$, the output value detected by the detector, is equal to the transmissivity T_i we mentioned before. Meanwhile, the pattern $I_1(x, y, t_i)$ stands for the result that the light

source intensity multiplies a mask modulation function A_i. Therefore, the correlation process[2] is

$$G^{(2)}_{\text{traditional}} = <I_1(x,y,t_i)I_2(t_i)> = <A_i T_i>. \quad (6)$$

However, the intensity of light source varies under the feedback loop, as shown in Eq. (3).

In this case, the pattern P_i, on the screen is $A_i \times I_i$ and the same pattern P_i, after the BS, also illuminates the object. When watching the screen, the eyes will integrate the patterns thanks to the vision persistence effect. So, the correlation between A_i and I_i is realized, and we mark this naked-eye ghost imaging result as

$$\hat{G}^{(2)} = <A_i I_i> = <P_i> = \int_t^{t+\tau} P_i \mathrm{d}t, \quad (7)$$

where τ is a limited time duration for integration. As a result, a negative image of Eq. (6) can be obtained via Eq. (7).

Here, the background introduced by the reference beam is still an obstacle to obtaining a good naked-eye ghost imaging result. A special pattern-scanning architecture designed on a low-speed light-modulation mask was proposed in our previous work[26] that can solve this problem. In our current work, we exploit this idea for such a system and introduce it briefly.

First, the object is divided into several blocks. Thus, the dimensionality of the image can be reduced. For instance, one can divide the object $(n \times n)$ into k column blocks. Every block is with $n \times (n/k)$ pixels.

Next, we use a complete set of low-order Hadamard scanning patterns to scan each block row by row, as shown in Fig. 2. So, one can get the visibility of each row in the block via this imaging method.

$$\text{Contrast}_{\hat{H}\_\text{Block}} = \frac{1 + N_{\text{Block}}}{1 + N_{\text{Block}}(2N_{\text{Block}} - 5)},$$
$$N_{\text{Block}} = n/k. \quad (8)$$

In order to get a high contrast via the Hadamard pattern, apart from sample scanning, it is a suitable choice that one can take $N_{\text{Block}} = 7$. In addition to the high contrast property, this method enables high-resolution imaging with lower-order Hadamard vectors and also boosts the imaging speed.

Figure 3 shows the work flowchart of the negative feedback digital modulation system. The output signal B of the bucket detector goes into this comparator to generate a TTL signal triggering the laser driver to modulate the laser intensity. In detail, when $I > b/T$, I will decrease to off. When $I < b/T$, I will increase to on, where b is the reference voltage. In this case, the laser intensity will approximate

$$I \approx \frac{b}{T}. \quad (9)$$

Figure 4 shows the high contrast imaging results ("X", "J", "T", and "U", respectively) obtained under the digital negative feedback loop.

Figure 5 shows the work flowchart of the negative feedback analog modulation system, which can also be expressed in Eq. (10). The feedback signal S from this analog modulator, controlling the laser, is the result that the reference voltage U minus the bucket detector's signal B:

$$S = I = U - B = U - I \times T. \quad (10)$$

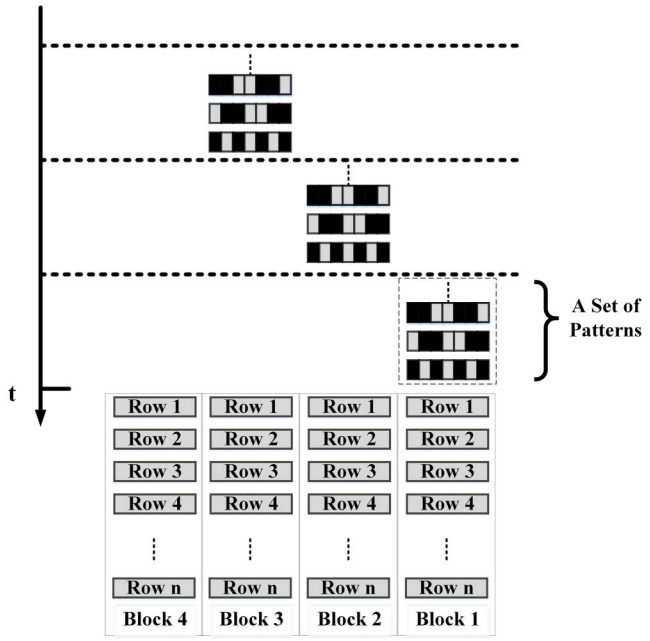

Fig. 2. Structure of the light modulation mask based on the Hadamard vector.

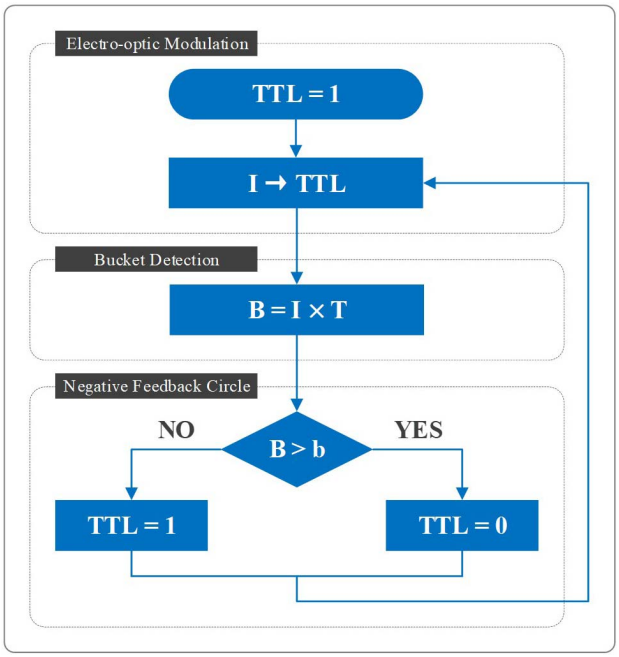

Fig. 3. Work flowchart for the negative feedback digital modulation system.

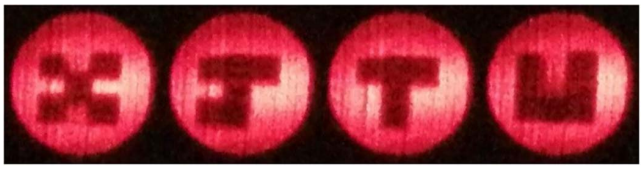

Fig. 4. Imaging result under digital negative feedback.

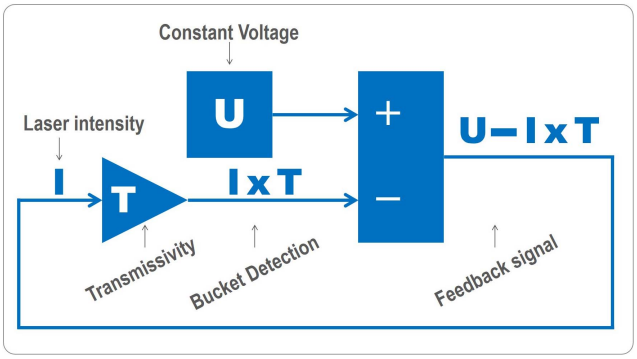

Fig. 5. Negative feedback loop of an analog modulation.

This signal is used to modulate the laser intensity. By solving $I = U - I \times T$ in Eq. (10), one gets

$$I = \frac{U}{\hat{T}}, \quad \hat{T} = 1 + T. \tag{11}$$

Figure 6 shows the high-contrast imaging results ("X", "J", "T", and "U", respectively) obtained by the analog negative feedback loop.

First, in the digital feedback loop, the noise signal from the ambient noise light or others will be limited by the digital modulator comparator. Moreover, if the noise goes through the comparator, the noise signal will be automatically suppressed via the negative feedback system.

Second, as well as the digital feedback loop, the analog feedback loop makes the output play the opposite role to the input of the noise, reducing the error between the system output and the system target. Ultimately, it makes the system tend to be stable.

Moreover, this feedback scheme can be better justified by the correspondence ghost imaging technique[27], and the image quality could be good with an appropriate threshold[28] or with AC coupling under different conditions, especially when the background is quite intense.

If the noise has been introduced into the system, the imaging expression will become

Fig. 6. Imaging result under analog negative feedback.

$$G_I^{(2)} = A_{N\times M}^T \left(\frac{b}{T - \Delta T_{\text{noise}}}\right)_{M\times 1}, \tag{12}$$

where N is the total number of pixels for imaging and M is the sampling numbers. Then, the Taylor expansion for Eq. (12) is

$$G_I^{(2)} = A_{N\times M}^T \left\{\frac{b}{T}\left[1 + \left(\frac{\Delta T_{\text{noise}}}{T}\right) + \left(\frac{\Delta T_{\text{noise}}}{T}\right)^2 + O\left(\frac{\Delta T_{\text{noise}}}{T}\right)^3\right]\right\}_{M\times 1}, \tag{13}$$

$$\left(\frac{\Delta T_{\text{noise}}}{T}\right)^n \ll \frac{\Delta T_{\text{noise}}}{T} \ll 1, \quad n \in \mathbf{N}^*. \tag{14}$$

Because ΔT_{noise} is much smaller than T, from Eq. (13) and Eq. (14), the effect of noise is significantly weakened.

From the imaging system, the modulator from projecting the object can be expressed as $A \times X$,

$$T_{M\times 1} = A_{N\times M}^T X_{N\times 1}, \tag{15}$$

where A is the mask modulation function and X denotes the object. Equation (1) can be rewritten via Eq. (15),

$$B_{M\times 1} = \text{diag}(I_{M\times 1}) A_{N\times M}^T X_{N\times 1}. \tag{16}$$

On the other hand, through Eq. (1), T is equal to the bucket signal value when the laser intensity is constant. So, the traditional correlated imaging can be obtained via T and A:

$$G^{(2)} = A_{N\times M}^T T_{M\times 1}. \tag{17}$$

However, the value of T is unknown, and only the laser intensity is changed with T. In addition, from Eq. (9) and Eq. (11), I and T are anti-related.

As shown in Fig. 1, while watching the screen, the human eye will automatically integrate the intensity modulated pattern. So, the imaging process can be expressed as

$$G_{I_1}^{(2)} = A_{N\times M}^T I_{M\times 1} = A_{N\times M}^T \left(\frac{b}{T}\right)_{M\times 1},$$
$$G_{I_2}^{(2)} = A_{N\times M}^T I_{M\times 1} = A_{N\times M}^T \left(\frac{U}{\hat{T}}\right)_{M\times 1}. \tag{18}$$

From Eq. (9) and Eq. (11), if the pattern speckle is very different from the object, the value of T is very small. Thus, the signal coming back is very weak and the bucket value B is very small too. Hence, the system will automatically increase the intensity of the current speckle via the simple feedback system we proposed. Conversely, it will automatically decrease the intensity of the current speckle. As a result, the principal component of the negative image is strengthened.

In conclusion, naked-eye ghost imaging via photoelectric feedback is realized. The obstacle to realizing

high-contrast real-time imaging for moving objects is removed by a special pattern-scanning architecture and a feedback system. Meanwhile, the high resolution and the boosted imaging speed can be obtained with a low pixel illumination from a low-speed rotating light-modulation mask. Two types of feedback circuits, digital and analog, are used to modulate the laser intensity, which will give the advantage of anti-noise. This work opens a new way to utilize ghost imaging that has a potential application to 3D ghost imaging visualization, ghost imaging virtual reality, single-photon imaging, and so on.

This work was supported by the Shaanxi Key Research and Development Project (No. 2019ZDLGY09-10), the Key Scientific and Technological Innovation Team of Shaanxi Province (No. 2018TD-024), the National Basic Research Program of China (973 Program) (No. 2015CB654602), and the 111 Project of China (No. B14040).

References

1. T. B. Pittman, Y. H. Shih, D. V. Strekalov, and A. V. Sergienko, Phys. Rev. A **52**, R3429 (1995).
2. A. Gatti, E. Brambilla, M. Bache, and L. A. Lugiato, Phys. Rev. Lett. **93**, 093602 (2004).
3. A. Gatti, E. Brambilla, M. Bache, and L. A. Lugiato, Phys. Rev. A **70**, 013802 (2004).
4. F. Ferri, D. Magatti, A. Gatti, M. Bache, E. Brambilla, and L. A. Lugiato, Phys. Rev. Lett. **94**, 183602 (2005).
5. A. Valencia, G. Scarcelli, M. D'Angelo, and Y. Shih, Phys. Rev. Lett. **94**, 063601 (2005).
6. D. Zhang, Y. H. Zhai, L. A. Wu, and X. H. Chen, Opt. Lett. **30**, 2354 (2005).
7. J. H. Shapiro, Phys. Rev. A **78**, 061802 (2008).
8. Y. Bromberg, O. Katz, and Y. Silberberg, Phys. Rev. A **79**, 053840 (2009).
9. D. Pelliccia, A. Rack, M. Scheel, V. Cantelli, and D. M. Paganin, Phys. Rev. Lett. **117**, 113902 (2016).
10. H. Yu, R. Lu, S. Han, H. Xie, G. Du, T. Xiao, and D. Zhu, Phys. Rev. Lett. **117**, 113901 (2016).
11. A. Schori and S. Shwartz, Opt. Express **25**, 14822 (2017).
12. A. X. Zhang, Y. H. He, L. A. Wu, L. M. Chen, and B. B. Wang, Optica **5**, 374 (2018).
13. R. I. Khakimov, B. M. Henson, D. K. Shin, S. S. Hodgman, R. G. Dall, K. G. Baldwin, and A. G. Truscott, Nature **540**, 100 (2016).
14. S. Li, F. Cropp, K. Kabra, T. J. Lane, G. Wetzstein, P. Musumeci, and D. Ratner, Phys. Rev. Lett. **121**, 114801 (2018).
15. T. Setala, T. Shirai, and A. T. Friberg, Phys. Rev. A **82**, 043813 (2010).
16. T. Shirai, T. Setala, and A. T. Friberg, J. Opt. Soc. Am. B **27**, 2549 (2010).
17. F. Devaux, P. A. Moreau, S. Denis, and E. Lantz, Optica **3**, 698 (2016).
18. P. Ryczkowski, M. Barbier, A. T. Friberg, J. M. Dudley, and G. Genty, Nat. Photonics **10**, 167 (2016).
19. S. Denis, P. A. Moreau, F. Devaux, and E. Lantz, J. Opt. **19**, 034002 (2017).
20. F. Devaux, K. P. Huy, S. Denis, E. Lantz, and P. A. Moreau, J. Opt. **19**, 024001 (2017).
21. J. Liu, J. Wang, H. Chen, H. Zheng, Y. Liu, Y. Zhou, F.-L. Li, and Z. Xu, Opt. Commun. **410**, 824 (2018).
22. H. Guo, R. Y. He, C. P. Wei, Z. Q. Lin, L. Wang, and S. M. Zhao, Chin. Opt. Lett. **17**, 071101 (2019).
23. X. Mei, C. Wang, Y. Fang, T. Song, W. Gong, and S. Han, Chin. Opt. Lett. **18**, 042602 (2020).
24. H. Zheng, G. Wang, Y. Zhou, J. Liu, H. Chen, and Z. Xu, China Patent ZL201710662518.5 (2020).
25. A. Boccolini, A. Fedrizzi, and D. Faccio, Opt. Express **27**, 9258 (2019).
26. G. Wang, H. Zheng, Y. Zhou, H. Chen, J. Liu, Y. He, Y. Yuan, F. Li, and Z. Xu, Sci. Rep. **10**, 2493 (2020).
27. K.-H. Luo, B.-Q. Huang, W.-M. Zheng, and L.-A. Wu, Chin. Phys. Lett. **29**, 074216 (2012).
28. J. Li, B. Luo, D. Yang, L. Yin, G. Wu, and H. Guo, Sci. Bull. **62**, 717 (2017).